ACS OMEGA

http://pubs.acs.org/journal/acsodf

Article

Using Amphiphilic Polymer Micelles as the Templates of Antisolvent Crystallization to Produce Drug Nanocrystals

Jianghao Zhang,[‖] Boxuan Lou,[‖] Xiaolan Qin, Yinwen Li, Haikuan Yuan, Lijuan Zhang, Xijian Liu, Yan Zhang, and Jie Lu*

Cite This: *ACS Omega* 2022, 7, 21000−21013

Read Online

ACCESS | Metrics & More | Article Recommendations | Supporting Information

ABSTRACT: Biocompatible and biodegradable amphiphilic polymeric micelles (PLA-CMCS-g-OA) were prepared by surface grafting of oleic acid and polylactic acid onto carboxymethyl chitosan and were used as templates for the crystallization of camptothecin. The camptothecin (CPT) nanocrystals prepared by the novel micelle-templated antisolvent crystallization (mt-ASC) method demonstrated higher crystallinity, narrower particle size distribution, and slower release characteristic than those prepared by conventional antisolvent crystallization (c-ASC) using a high initial concentration and fast addition rate. In particular, the CPT release behavior of mt-ASC products in phosphate buffer solutions presented a pH-responsive characteristic with the increasing release rate of CPT under lower pH conditions. This work confirmed that amphiphilic nanomicelle-templated crystallization was an effective method for preparing drug nanocrystals.

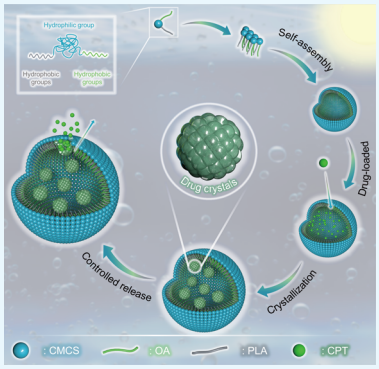

1. INTRODUCTION

Nanometerization of drug crystals is a robust approach to improve their solubility and bioavailability.[1,2] Over the last decade, extensive research has been carried out to prepare nanocrystals of various pharmaceuticals for increased solubility, outstanding reproducibility, and excellent patient compliance.[3] So far, both top−down and bottom−up methods have been utilized to prepare drug nanocrystals.[4,5] A top−down approach, which generally includes media grinding and high-pressure homogenization, relies on mechanical forces to reduce large crystalline particles in the millimeter/micron scale to nanoparticles,[6,7] whereas a bottom-up approach involves the formation of drug nanocrystals from solutions of ions or molecules through synthesis or self-assembly,[8] including rapid precipitation (reaction or antisolvent crystallization), supercritical fluid crystallization, water (solvent) thermal synthesis, microemulsion, solvent volatilization, etc.[9] Because it is simple and easy to scale up, the traditional top−down method has been commercialized. Nonetheless, due to the use of external force to crush the crystal, the method suffers from some inherent drawbacks, i.e., incomplete structure of products, poor product purity, etc.[10] Though it is scarcely commercialized, the bottom−up method exhibits the advantages of less energy demanding and high product purity.[11] Prof. Chen's group has successfully developed the supergravity precipitation method to prepare ultrafine drug crystals such as sorafenib and itraconazole.[12,13] Zhao et al.[14] have adopted precipitation-combined high-pressure homogenization technology to prepare hydroxycamptothecin nanosuspensions. Although rapid precipitation is able to produce drug nanoparticles, its products normally exhibit low crystallinity and wide particle size distribution (PSD) stemming from the fast homogeneous nucleation rate. Therefore, it is necessary to exploit novel crystallization technologies for better product quality.

Currently, multifarious inorganic and organic templates have been employed in the preparation of various nanomaterials.[15] Nanocrystallization mediated by templates can be expected to control the size, shape, structure, and property of nanocrystals,[16] which accordingly solves the problems of incomplete structure, uneven particle size, unstable dispersion, and poor crystallinity of the products by using current methods.[17]

Amphiphilic polymers, consisted of hydrophobic and hydrophilic segments, have been extensively utilized to construct micelles with various structures by self-assembly.[18] Today, most of the amphiphilic polymer micelles are employed in cancer treatment as drug delivery systems.[19] In particular, stimulus-responsive polymer micelles are known as the most valuable and extensively studied as carriers for nanomedicine where they are generally deemed to play important roles in the drugs' controlled release.[20] For examples, Fang and co-workers[21] have successfully developed a simple method for assembling dual-stimuli polymeric micelles PEG-PBA-TGMS to deliver dexamethasone for arthritis. Teng and co-workers[22]

Received: March 24, 2022
Accepted: May 27, 2022
Published: June 7, 2022

have synthesized biofriendly amphiphilic polymers mPEG-PCADK and mPEG-PK3 to deliver superoxide dismutase. From these studies, it can be anticipated that amphiphilic polymer micelles maybe a good choice for drug crystallization templates, which are not only simple to prepare but also have good biocompatibility and low toxicity.[23,24]

Carboxymethyl chitosan (CMCS), widely used in the pharmaceutical industry, is one of the derivatives of chitosan (CS) that are solubilized over a wide range of pH. Due to its good solubility in water, CMCS is now frequently employed as a drug carrier in biomedical fields. It contains $-NH_2$ and $-COOH$ groups, which are versatile and pH-responsive, providing a way to prepare pH-responsive nanomicelles.[25] Oleic acid (OA) possesses high hydrophobicity and good antitumor activity.[26] Polylactic acid (PLA), an aliphatic polyester, is a functional polymer material with good biocompatibility and biodegradability and is often applied in drug delivery systems, tissue engineering, surgical sutures, etc.[18] In this work, an amphiphilic polymer PLA-CMCS-g-OA has been first constructed using three biocompatible and degradable materials of OA, PLA, and CMCS. The new polymer is formed by grafting of two hydrophobic blocks, which endow its micelles with an increased loading capacity for the hydrophobic anticancer drug camptothecin (CPT) up to 17.22%. The nanosized normal-phase micelles are prepared by dispersing its concentrated DMSO solutions into appropriate amounts of water under vigorous stirring. The morphology of micelles is observed by transmission electron microscopy (TEM), and the stability of micelles at different temperatures is investigated by using dynamic light scattering (DLS). Meanwhile, the self-assembly of PLA-CMCS-g-OA micelles is simulated using dissipative particle dynamic (DPD) simulations. The morphology of blank micelles predicted by DPD was consistent with that observed by TEM. Then, the PLA-CMCS-g-OA micelles are used as the template of the antisolvent crystallization of poorly soluble CPT to prepare its nanocrystals. Finally, the CPT release profiles of the obtained nanoproducts under different pH conditions have been investigated.

2. SIMULATIONS

Both the calculation of solubility parameters and the process simulation of micelle self-assembly were carried out by Materials Studio 7.0.[27]

2.1. Solubility Parameters. First, the structures of the CMCS monomer, the hydrophobic segment OA, and the PLA monomer were geometrically optimized using the Forcite module. The force field was set as COMPASS. The methods of atom-based and Ewald were adopted for acquiring the forces of van der Waals and Coulomb, respectively.[28] Then, 50 segments or monomers of above each structure were energetically minimized in Amorphous Cell. After this, molecular dynamic simulations were carried out for the obtained three cells using the Forcite module.[29] The *NVT* ensemble was selected for the generation of trajectories under a constant particle number, cell volume, and temperature (25 °C). The time of simulation and step were 1000 ps and 1 fs, respectively, each frame was delivered every 1000 steps, and the pressure control method was Berendsen. Finally, the solubility parameter (δ) of each structure was obtained through the trajectory after equilibrium (2000−4000 ps) using the Forcite module.[30] Thus, the Flory−Huggins parameter (χ_{ij}) was calculated by[31]

$$\chi_{ij} = \frac{(\delta_i - \delta_j)V_b}{RT} \quad (1)$$

where V_b refers to the mean value of the molar volumes of structures i and j.

The repulsive parameter (a_{ij}) as listed in Table 1 was calculated by[32]

$$a_{ij} = a_{ii} + 3.5\chi_{ij} \quad (2)$$

where a_{ii} is equal to 25.00.

Table 1. Interaction Parameters (a_{ij}) Obtained

structure	O (OA)	L (LA)	M (CMCS)	W (water)
O (OA)	25.00			
L (LA)	58.52	25.00		
M (CMCS)	30.64	34.79	25.00	
W (water)	95.42	93.80	99.73	25.00

2.2. Micelle Self-Assembly. The self-assembly process of PLA-CMCS-g-OA micelles was simulated by DPD, in which the constructed coarse-grained model is shown in Figure 1.

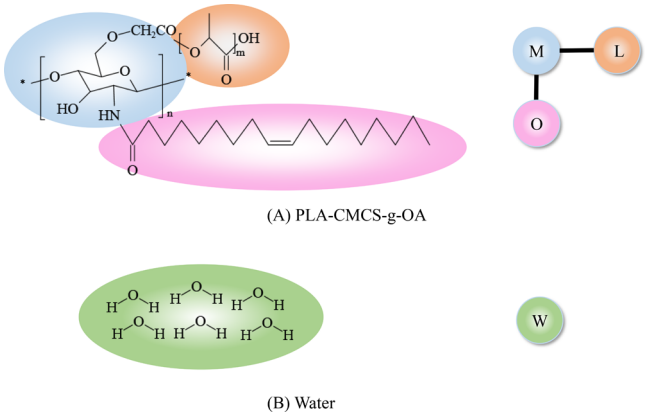

Figure 1. Coarse-grained beads of (A) PLA-CMCS-g-OA and (B) water.

PLA-CMCS-g-OA had been split into three kinds of beads, i.e., PLA (orange), CMCS (blue), and OA (pink). Meanwhile, each water bead (green) included six water molecules. According to the method described in the literature,[33] a 30 × 30 × 30 r_c^3 simulation box was first filled randomly with the PLA-CMCS-g-OA and water coarse-grained beads at a number ratio of 3 to 80 to form the initial model of PLA-CMCS-g-OA aqueous solution using the mesostructure. The number ratio of beads PLA, CMCS, and OA was 1:1:1, and r_c (cut-off radius) was set as 1. Then, the initial model was simulated by DPD to obtain the dynamic evolution of PLA-CMCS-g-OA micelles in water. The force field was COMPASS, and the temperature was 25 °C with the density of beads being set as 3. The step time and the spring constant were set as 0.05 ns and 4.0, respectively. The total number of steps in the simulation was 100,000, which was larger than 83,000 required for reaching the equilibrium state.

3. RESULTS AND DISCUSSION

3.1. Characterization of Intermediate and Final Amphiphilic Polymers. Figure 2 presents the infrared spectra of three materials and two polymer products. As to

https://doi.org/10.1021/acsomega.2c01792
ACS Omega 2022, 7, 21000−21013

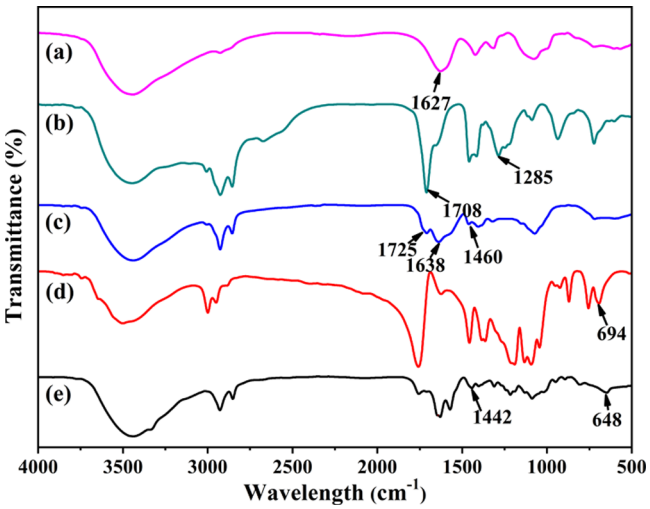

Figure 2. FTIR spectra of (a) CMCS, (b) OA, (c) CMCS-g-OA, (d) PLA, and (e) PLA-CMCS-g-OA.

CMCS, OA, and CMCS-g-OA, the peak at 1285 cm^{-1}, which is certainly related to the stretching vibration of carbon−oxygen single bonds in the carboxyl group of OA, is not found in the spectrum of CMCS-g-OA, implying that −OH has been removed from the carboxyl group when OA reacts with CMCS. Meanwhile, the peak at 1627 cm^{-1}, which should be related to the bending vibration of nitrogen−hydrogen bonds in the amino group of CMCS, and the peak at 1708 cm^{-1}, which should be related to the stretching vibration of carbon−oxygen double bonds in the carboxyl group of OA, hypochromatically shift to 1638 and 1725 cm^{-1}, respectively, which further proves the formation of amide bonds between CMCS and OA.[26,34]

By comparing the spectra of CMCS-g-OA, PLA, and PLA-CMCS-g-OA, the peak at 1460 cm^{-1}, which is concerned with the in-plane bending of carbon−hydrogen single bonds adjacent to the carboxyl group of CMCS-g-OA, bathochromically shifts to 1442 cm^{-1}. Meanwhile, the peak at 694 cm^{-1}, which should be related to the stretching of carbon−oxygen single bonds adjacent to the carbonyl group of PLA, also bathochromically shifts to 648 cm^{-1}. All the results from Fourier transform infrared spectroscopy (FTIR) confirm that CMCS-g-OA and PLA-CMCS-g-OA have been successfully fabricated.

Figure 3 presents the ^{1}H NMR spectra of three materials and two polymer products. In all spectra, the peak at 7.28 ppm is the characteristic shift of the deuterated chloroform solvent. The peaks at 3.0−4.0 ppm are assigned to the ring methine protons of CMCS. The spectrum of OA shows a peak at 5.30 ppm assigned to the olefinic protons (alkene protons), and the corresponding signals of the remaining protons are below 3.0 ppm. At the same time, the peaks at 5.36, 2.01, and 0.8 to 0.9 ppm assigned to the proton shifts of olefin, methylene, and terminal methyl, respectively, are present in the spectrum of CMCS-g-OA.[26] ^{1}H NMR results prove that OA has been successfully grafted onto CMCS. The peaks at 5.16 and 5.36 ppm can be assigned to the methylene proton in the repeating unit of PLA and the olefin proton of OA, respectively, and both peaks are observed in the spectrum of PLA-CMCS-g-OA, confirming that PLA has been successfully grafted onto CMCS-g-OA.[18] Besides, the contents of OA and PLA in PLA-CMCS-g-OA estimated from the proton integral intensity ratios are ca. 13.56 and 16.19%, respectively, and the yields of CMCS-g-OA and PLA-CMCS-g-OA are 63.87 and 60.51%, respectively.

The molecular weights based on mass average (M_w) and number average (M_n) as well as their ratios (M_w/M_n) of CMCS-g-OA and PLA-CMCS-g-OA are shown in Table 2. The gel permeation chromatographic (GPC) spectra of two in-house synthesized polymers are supplemented in Figure S1 (Supporting Information). Both polymers exhibit a narrow molecular weight distribution as evinced by M_w/M_n within the range of 1.1−1.2.

The TGA/DTG curves of CMCS, CMCS-g-OA, and PLA-CMCS-g-OA under a nitrogen atmosphere are shown in Figure 4. It can be observed that the first stage of weight loss is concerned with the solvent evaporation and the significant weight loss starting from 230, 210, and 160 °C is deemed as a decomposition of CMCS, CMCS-g-OA, and PLA-CMCS-g-OA, respectively.[35]

3.2. Critical Micelle Concentration. Figure 5 illustrates the I_1/I_3 ratios of pyrene versus the concentrations of CMCS-g-OA and PLA-CMCS-g-OA in water. From the two intersection points, the critical micelle concentration (CMC) is found to be 0.036 mg/mL for CMCS-g-OA and 0.030 mg/mL for PLA-CMCS-g-OA. The lower CMC of PLA-CMCS-g-OA may be because the latter has been grafted with another hydrophobic fragment of PLA, endowing the former with a higher capability to form micelles in water.[36]

3.3. Characterization of Blank Micelles. The PSD values of CMCS-g-OA and PLA-CMCS-g-OA micelles measured by DLS are shown in Figure 6A. The average size, zeta potential (Z), and polydispersity index (PDI, here defined as $(\sigma/\overline{d})^2$; $\overline{d}$ is the mean hydrodynamic diameter, and σ is the standard deviation) of blank CMCS-g-OA and PLA-CMCS-g-OA micelles are listed in Table 2. The CMCS-g-OA micelles present a bimodal distribution, with large micelles appearing at about 700 nm, indicating that some micelles can form aggregates. The average size of unaggregated micelles is 87.8 ± 3.58 nm. The PLA-CMCS-g-OA micelles demonstrate a unimodal distribution with an average size of 112.4 ± 4.36 nm. The grafting of hydrophobic PLA onto CMCS-g-OA makes PLA-CMCS-g-OA more hydrophobic and increases the hydrophobic chamber of the micelles.[36]

The morphologies of the dried CMCS-g-OA and PLA-CMCS-g-OA micelles negatively stained with phosphotungstic acid observed by TEM are shown in Figure 6B,C. Both dried blank CMCS-g-OA and PLA-CMCS-g-OA micelles maintain spherical-like shapes with average sizes of ca. 70.0 and 100.0 nm, respectively. It is obvious that the size of dried blank micelles is generally smaller than that in water because the size measured by DLS refers to the hydraulic diameter, and the naturally dried micelles undergo a process of shrinkage.[35] As shown in Figure 6D, the outline of the micelles can be clearly observed, where the pale color part is the hydrophilic shell (wall) of the micelles with a thickness of ca. 11.60 nm and the deep black part is the hydrophobic cavity of the micelles.[26,37,38] More exact microstructure information of micelles may be acquired through wide-angle and small-angle X-ray scattering.

3.4. DPD Simulation. Figure 7 shows the snapshots of a dynamic self-assembly of PLA-CMCS-g-OA blank micelles at different steps. The water beads are not displayed in Figure 7 for a clear observation of the morphology of self-assembling aggregates. DPD simulation results indicate that the polymer molecules in water start to self-assemble when the number of

https://doi.org/10.1021/acsomega.2c01792
ACS Omega 2022, 7, 21000−21013

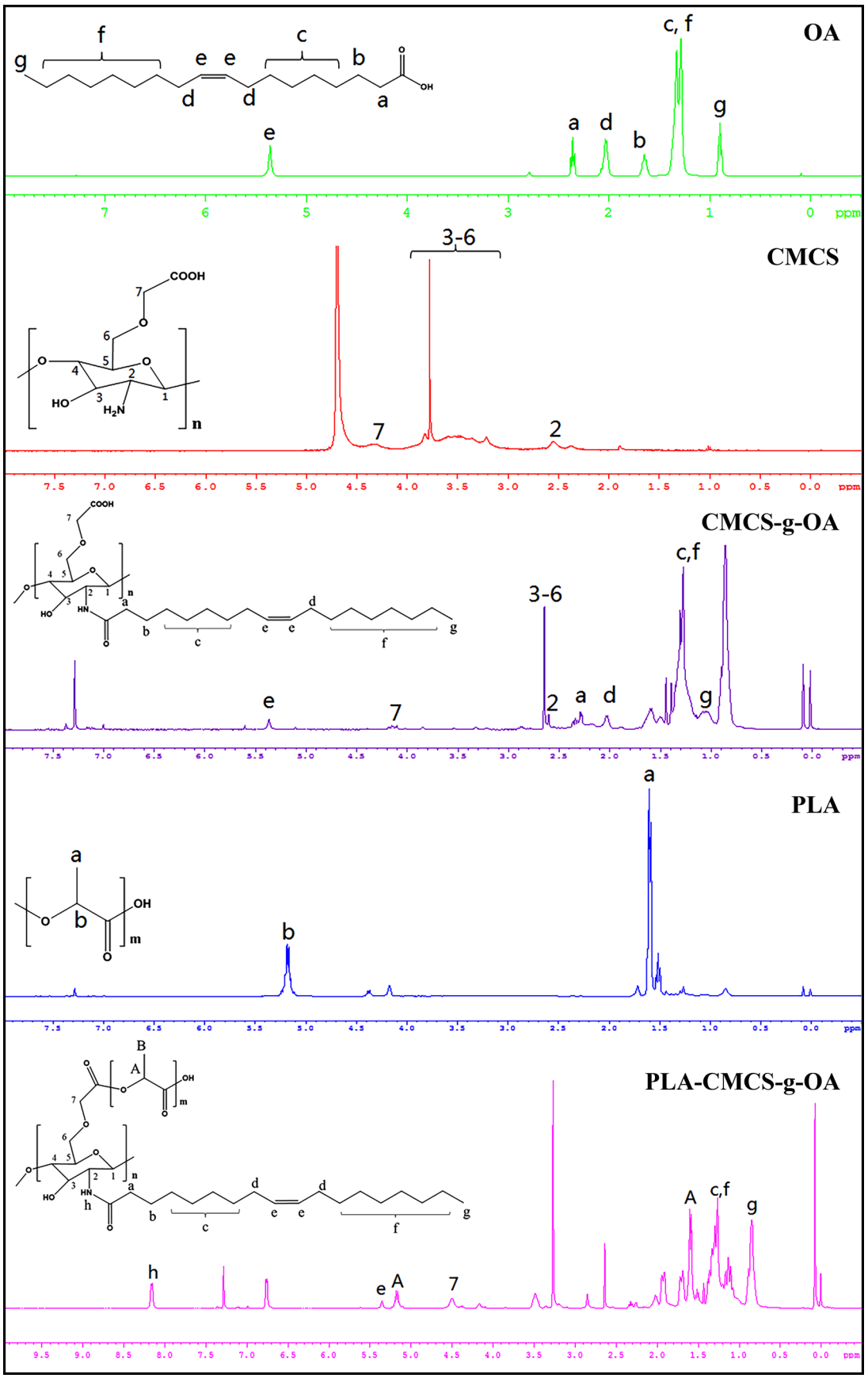

Figure 3. [1]H NMR spectra from OA, CMCS, CMCS-g-OA, PLA, and PLA-CMCS-g-OA.

https://doi.org/10.1021/acsomega.2c01792
ACS Omega 2022, 7, 21000−21013

Table 2. Molecular Weight, Average Size, and Zeta Potential

	polymers			blank micelles		
	M_n	M_w	M_w/M_n [a]	$\bar{d}$ (nm)	PDI [b]	Z (mV)
CMCS-g-OA	15,300	16,864	1.10	87.8 ± 3.58	0.196	−25.7 ± 6.45
PLA-CMCS-g-OA	23,972	26,879	1.12	112.4 ± 4.36	0.142	−28.6 ± 2.78

[a]Measured by GPC. [b]Measured by DLS.

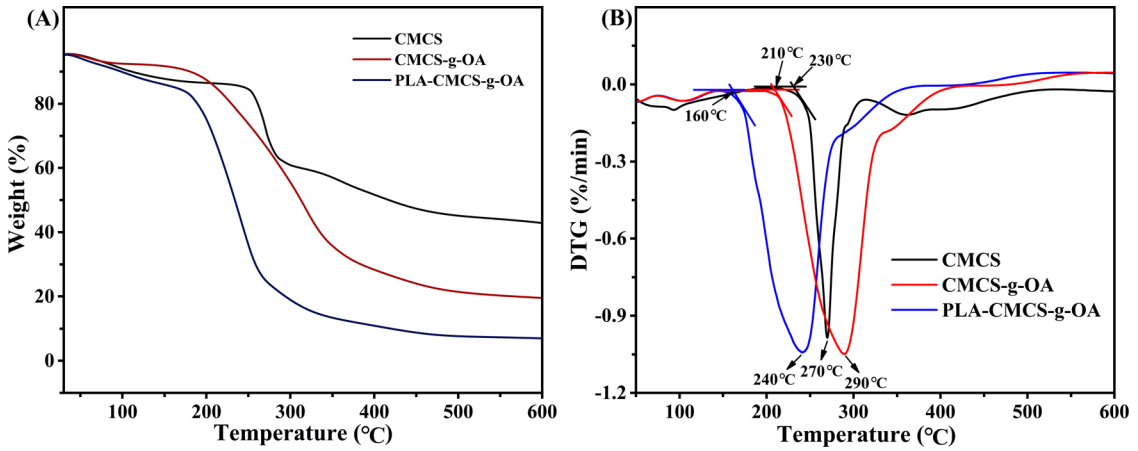

Figure 4. (A) TGA and (B) DTG curves of CMCS, CMCS-g-OA, and PLA-CMCS-g-OA.

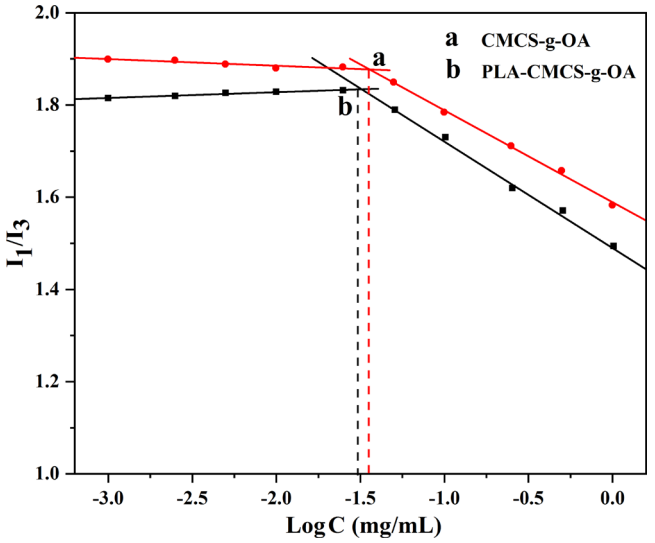

Figure 5. Plotting I_1/I_3 of pyrene versus concentration levels of (a) CMCS-g-OA and (b) PLA-CMCS-g-OA in water.

steps is higher than 1000. However, when the number of steps reaches 15,000, the number of small micelles is apparently declined because they grow into the larger ones. As shown in Figure 7H, the system reaches equilibrium at 83,000 steps and the size and the number of micelles would no longer change.[30] The final morphology of simulated micelles is spherical, which is as the same as that observed by TEM.

3.5. Stability of PLA-CMCS-g-OA Blank Micelles. Good stability has been observed from the as-prepared PLA-CMCS-g-OA blank micelles. As shown in Figure 8A, the average sizes of PLA-CMCS-g-OA blank micelles are almost unchanged when they are stored at 4 or 37 °C over 1 week. Meanwhile, the PDI data (Figure 8B) slightly fluctuate within the range of 0.22−0.28. The results prove that the micelles self-assembled by hydrophobic/hydrophilic/hydrophobic polymers have an excellent stability in water under the studied temperature range.

3.6. Solubility. The molar fraction solubilities (X^*) of CPT in the mixed solvents of DMSO and water under atmospheric pressure at 25 °C are shown in Figure 9. It can be seen that the solubility of CPT in the mixed solvents decreases greatly with the increasing mass percentage of water, suggesting that water can be used as an antisolvent of the crystallization of CPT from its concentrated solution. Under the same temperature, the solubility of CPT in DMSO (1.58×10^{-3}) is higher than that in DMF (6.55×10^{-4}). The diffractograms of the residual solids of CPT in the studied solvents have been supplemented in Figure S2 (Supporting Information). All diffractograms of the remaining solids are the same as that of raw CPT, implying that there is no crystal form conversion during the solubility measurement.[39]

3.7. Drug Loading Capacity of Micelles. Table 3 lists the loading capacity (LC) for CPT of blank micelles and the average particle size as well as the PDI of CPT-loaded micelles. The size of CPT-loaded micelles is distinctly larger than those of blank micelles due to the hydrophobic repulsion. Similarly, the PDI of the micelles is increased when they are loaded by CPT. Furthermore, it is also found that the PLA-CMCS-g-OA micelles have an excellent capacity of CPT loading up to 17.22%, which exceeds the reported drug *LC*. Table 4 compares the size as well as the LC of synthesized CPT-loaded polymeric micelles with other micelles.

3.8. Characterization of CPT Products from c-ASC and mt-ASC. The powder X-ray diffraction (PXRD) diffractograms of crystallization products and raw CPT are compared in Figure 10. In general, the most prominent peak of all products can be found at 13.4 ± 0.1°. However, compared with the raw material, the peak intensity of the product obtained by c-ASC at an addition rate of 2 mL/min decreases to a certain extent, indicating that the crystallinity of the product is slightly decreased. Meanwhile, in the diffractogram of the product obtained by c-ASC with the linear addition, in addition to the

https://doi.org/10.1021/acsomega.2c01792
ACS Omega 2022, 7, 21000−21013

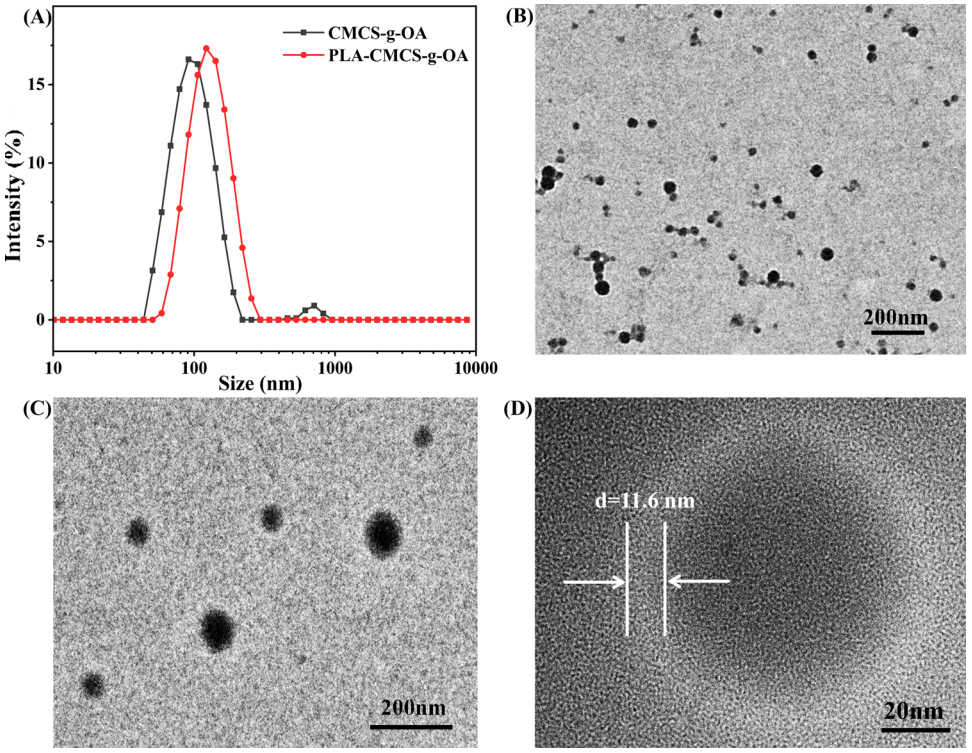

Figure 6. (A) Average sizes and TEM images of (B) CMCS-g-OA and (C,D) PLA-CMCS-g-OA blank micelles.

great peak number and intensity decline, there appear wide and large humps, indicating that the crystallinity of the product has been decreased significantly. Although the peak number and intensity of the mt-ASC product are smaller than those of the raw material, it still maintains good crystallinity as the decrease in the peak number and intensity should have been resulted from the reduction of crystal size and the presence of the amorphous polymer.[44]

As shown in Figure 11A, the raw CPT crystals are in the shape of micron-sized chunks. Meanwhile, as shown in Figure 11B, the size of particles obtained by c-ASC at an addition rate of 2 mL/min is about one-twentieth that of the raw material crystals, though few of them are in the nanoscale. At the same time, the particles obtained by c-ASC with the linear addition are in nanoscale size, but most of them are sticky agglomerates (Figure 11C). As shown in Figure 11D, the spherical-like particles obtained by mt-ASC are well dispersed without agglomeration. The inset at high TEM magnification illustrates that the CPT nanocrystals in the PLA-CMCS-g-OA micelles have a lattice distance of 0.17 nm. In brief, the CPT nanocrystals prepared by the template method possess more desirable and evenly distributed particle size, shape, and crystallinity than those prepared by conventional rapid crystallization and accordingly are more favorable for the release, absorption, and utilization of CPT.[35,45]

The stability of the mt-ASC product (i.e., CPT nanocrystal-loaded micelles) is shown in Figure 12, which is determined by DLS at 37 °C over 1 week. Generally, the large fluctuation of average size and PDI of CPT nanocrystal-loaded micelles in the first few days is attributed to the swelling of dried micelles and the dissolution of nanocrystals in them. Subsequently, the average size of CPT nanocrystal-loaded micelles decreases and then stays stable until reaching their equilibria.[46]

The templating mechanism of the amphiphilic polymer micelle upon the antisolvent crystallization is schematically illustrated in Figure 13. When the antisolvent molecules enter the CPT solution in the hydrophobic chamber of the micelle through molecular diffusion driven by the chemical potential, the solution gradually becomes supersaturated. On the surface of the hydrophobic chain, the adsorbed CPT molecules are gradually condensed and structurally rearranged through the relaxation of the chain, resulting in the heterogeneous primary nucleation of CPT crystals. Their diffusion-limited growth not only depends on the supply of supersaturation but also is confined by the size of the hydrophobic chamber.[47]

3.9. Drug Release. To investigate the pH sensitivity of CPT-loaded micelles, the size of the micelles in PBS with different pH within 12 h is measured by DLS. As shown in Figure 14A, the size of micelles does not change significantly in PBS at pH 7.4 within monitoring duration, while the sizes of micelles in PBS at pH 6.5 and 1.2 exhibit a noticeable increase, increasing from 164.0 to 295.0 nm and 255.0 to 1480.0 nm, respectively. It can be explained that the ester linkages between hydrophilic CMCS and hydrophobic PLA as well as the amide bond between CMCS and hydrophobic OA are broken in the acid environment, in turn causing the micelle disassembly.[48−51] Therefore, CPT-loaded micelles exhibit pH sensitivity, which will be conducive to the controlled release of drugs in the acidic environment.

Figure 14B,C respectively depicts the CPT release profiles of raw material and crystallization products in PBS at pH 7.4 and those of the mt-ASC product at pH 1.2, 6.5, and 7.4. Generally, at the same release time, the cumulative release amount of CPT from the c-ASC product using a linear addition is the largest, whereas that from the mt-ASC product is the smallest. After 48 h, 93.82, 83.24, and 46.03% of total CPT have been released from the particles of c-ASC, raw material, and mt-ASC under pH 7.4, respectively. In addition, the particles produced by mt-ASC show the pH-responsive characteristic to a certain degree. The release ratio of CPT increased with decreasing pH,

https://doi.org/10.1021/acsomega.2c01792
ACS Omega 2022, 7, 21000−21013

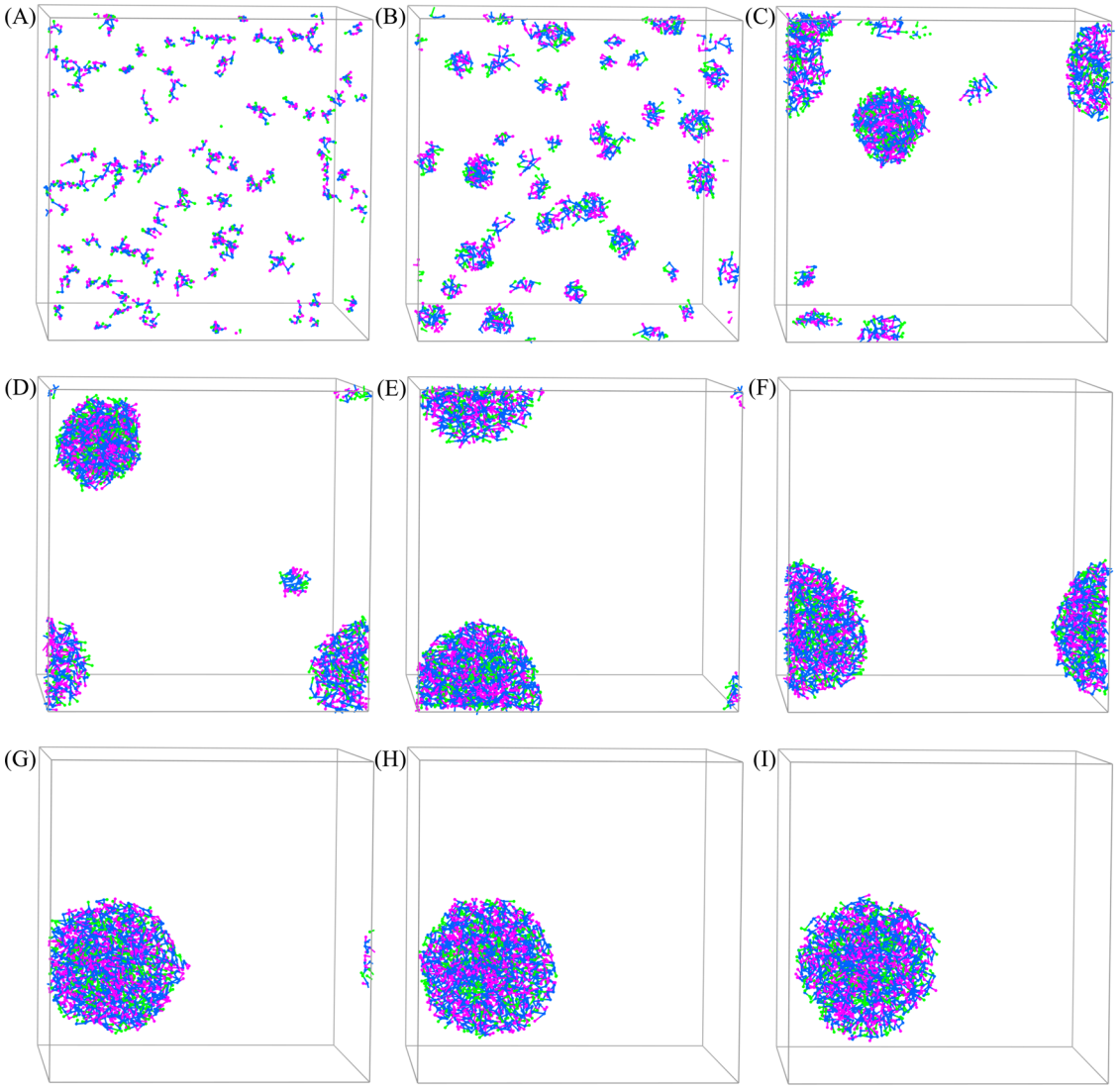

Figure 7. Snapshots of the evolution of PLA-CMCS-g-OA in water at simulation steps (A) 0, (B) 10^3, (C) 1.5×10^4, (D) 4×10^4, (E) 6×10^4, (F) 7×10^4, (G) 8×10^4, (H) 8.3×10^4, and (I) 10^5.

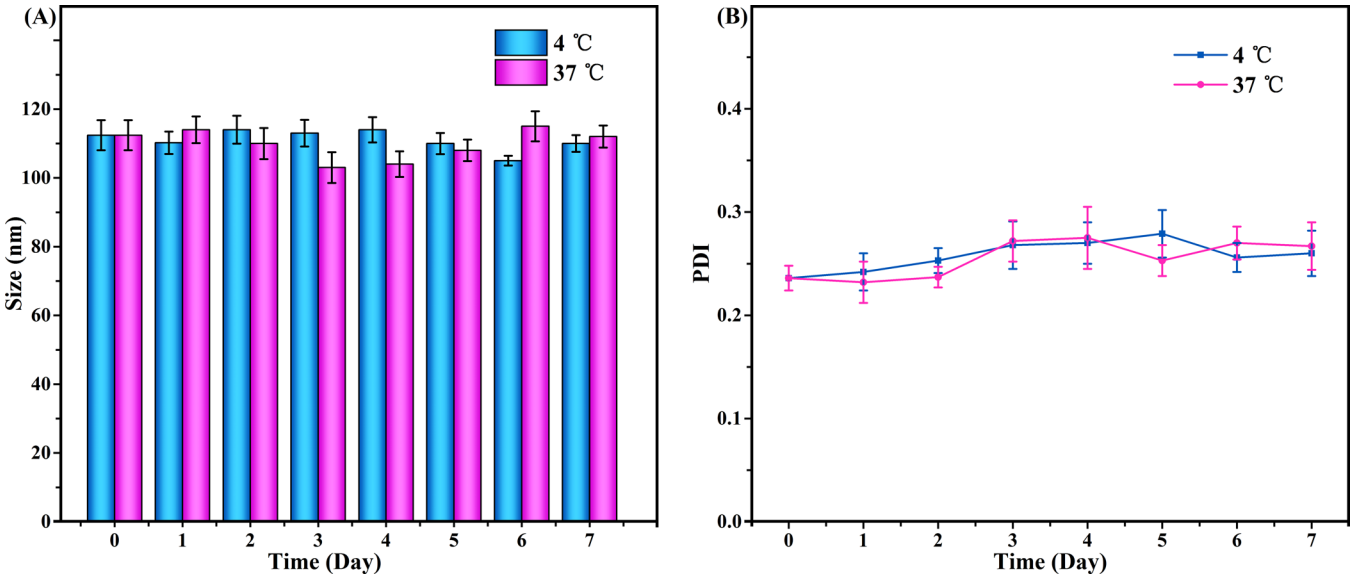

Figure 8. (A) Average size and (B) PDI of PLA-CMCS-g-OA blank micelles at 4 or 37 °C over 1 week.

https://doi.org/10.1021/acsomega.2c01792
ACS Omega 2022, 7, 21000−21013

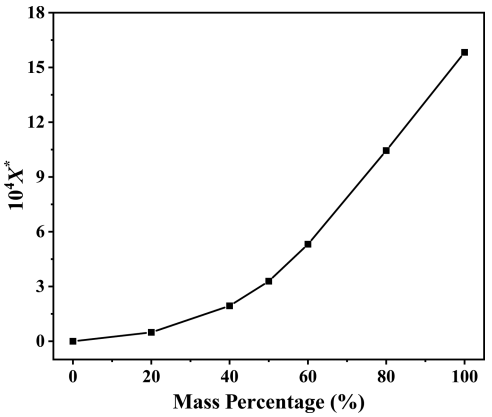

Figure 9. Experimental solubility of CPT in the mixed solvents of DMSO and water at 25 °C.

Table 3. Particle Size, PDI, Zeta Potential, and LC of CPT-Loaded PLA-CMCS-g-OA Micelles and Unloaded Micelles

polymer micelles	$\overline{d}$ (nm)	PDI	Z (mV)	LC (%)
unloaded PLA-CMCS-g-OA	112 ± 4.36	0.232	−28.6 ± 2.78	
CPT-loaded PLA-CMCS-g-OA	150 ± 3.67	0.289	−30.5 ± 3.90	17.22

Table 4. Comparison of Drug Loading Capacity of Various Micelles

polymer micelles	$\overline{d}$ (nm)	drug	LC (%)	refs
PDCAH	229.33	CPT	10.11	40
mPEG-CS-OA	146	CPT	5.0	31
PLGA-PEI	121	CPT	3.3	41
PEG-PCL	90−120	CPT	11.6	42
PEG_{114}-b-P($CAMA_{0.6}$-*co*-$ImOAMA_{0.4}$)$_{46}$	54.3	CPT	10.3	43
PLA-CMCS-g-OA	150	CPT	17.22	this work

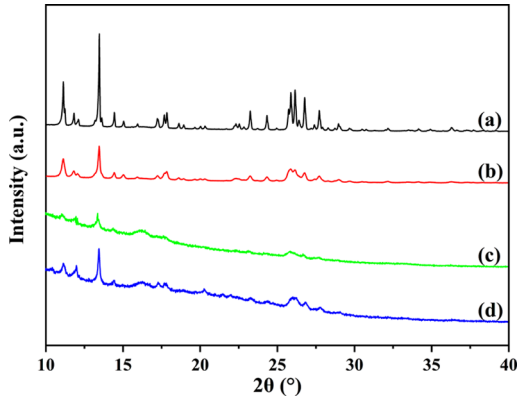

Figure 10. PXRD diffractograms of (a) raw CPT along with the products from (b,c) c-ASC and (d) mt-ASC.

which is owing to the acidic condition leading to disassembly of the micelles. In an acidic environment, the ester bond formed between PLA and CMCS and the amide bond between CMCS and OA are broken due to protonation, leading to a dissociation of PLA-CMCS-g-OA micelles and accordingly a fast release of CPT.[48−51] Meanwhile, erosion or degradation of micelles in acidic conditions may also bring about the faster drug release than in neutral environments.[52−54] According to the literature,[42,55] the micelles constructed of biocompatible PLA, CMCS, and OA shall reduce the cytotoxicity of CPT nanocrystals on normal cells, which can be further clarified through in vitro and in vivo studies. The standard curve of CPT in DMF is shown in the Supporting Information (Figure S3).

4. CONCLUSIONS

In this work, a novel amphiphilic micelle, PLA-CMCS-g-OA, was synthesized as a template for the antisolvent crystallization to prepare CPT nanocrystals. The LC of PLA-CMCS-g-OA polymer micelles was high up to 17.22% larger than that of the currently reported micelles. Moreover, it was particularly meaningful that the CPT nanocrystals prepared by amphiphilic nanomicelle-templated antisolvent crystallization possessed a uniform nanoparticle size, excellent dispersibility, high crystallinity, and desirable in vitro pH-responsive release profile. The work solidly proved that polymer micelles had a promising application prospect as templates for the crystallization to prepare the nanocrystals of drugs.

5. EXPERIMENTAL SECTION

5.1. Materials. OA, CMCS with a molecular weight range of 1.5×10^4 Da (degree of deacetylation ≥85% and degree of carboxymethyl ≥80%), PLA with a molecular weight of 2×10^3 Da, ethanol, 4-dimethylaminopyridine (DMAP, mass purity ≥99%), *N*,*N*′-dicyclohexylcarbodiimide (DCC, mass purity ≥99%), EDC (mass purity ≥99%), *N*-hydroxysuccinimide (NHS, mass purity ≥99%), *N*,*N*-dimethylformamide (DMF, mass purity ≥99%), dimethyl sulfoxide (DMSO, mass purity ≥99%), citric acid monohydrate (mass purity ≥99%), sodium phosphate dibasic dodecahydrate (mass purity ≥99%), and sodium phosphate monobasic dehydrate (mass purity ≥99%) were supplied from Titan High-Tech (Shanghai, China). Camptothecin (CPT, mass purity ≥97%) was purchased from Biochempartner (Shanghai, China). Deionized (DI) water was supplied from a PureUP device from Ulupure (Shanghai, China).

5.2. Syntheses of Amphiphilic Polymers. Two-step synthesis of PLA-CMCS-g-OA is illustrated in Scheme 1, in which the molecular structures were constructed and visualized by Materials Studio 7.0 software.[56] In the first step, CMCS-g-OA was synthesized by the amide reaction according to a previous study.[29] Specifically, 1.00 g (6.67×10^{-5} mol) of CMCS was dissolved in 60 mL of DI water at 80 °C to acquire a CMCS aqueous solution. Meanwhile, 1.56 g (5.52×10^{-3} mol) of OA, 0.96 g (8.34×10^{-3} mol) of NHS, and 1.58 g (1.02×10^{-2} mol) of EDC were added into 60 mL of ethanol, where the resulting mixture was stirred under 25 °C for 6 h to activate the carboxyl group of OA. The activated OA solution was then slowly dropped to the CMCS solution at 0.5 mL/min at 80 °C. Afterward, the obtained mixture was kept stirring for 5 and 12 h at 80 and 25 °C, respectively, followed by being dialyzed with DI water overnight for the removal of NHS and EDC through a JSK-T002 dialysis bag (MWCO 7×10^3 Da, Jisskang Biotechnology, Qingdao, China). Finally, the residuum in the bag was freeze-dried using an FD80AD lyophilizer (Bilon, Shanghai, China), and the obtained solids (CMCS-g-OA) were washed using ethanol to remove unreacted OA and dried in a vacuum for further use. Subsequently, the esterification reaction was adopted to

https://doi.org/10.1021/acsomega.2c01792
ACS Omega 2022, 7, 21000−21013

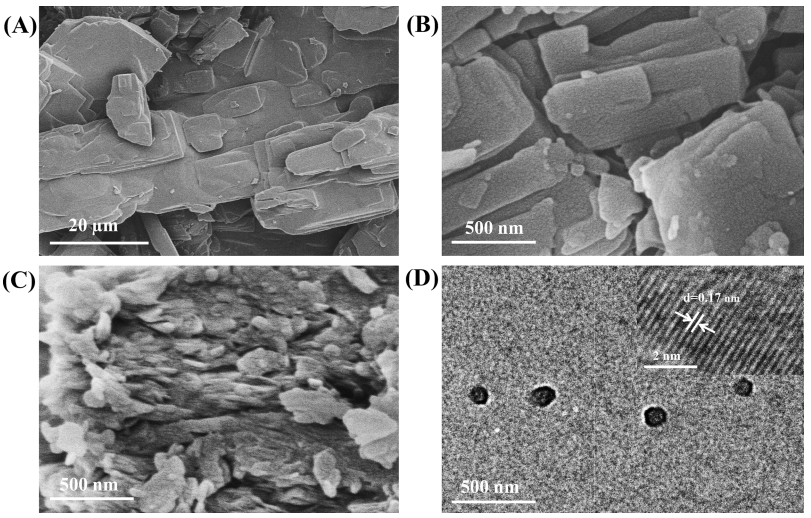

Figure 11. SEM images of (A) raw CPT and (B,C) c-ASC products and TEM images of (D) mt-ASC products.

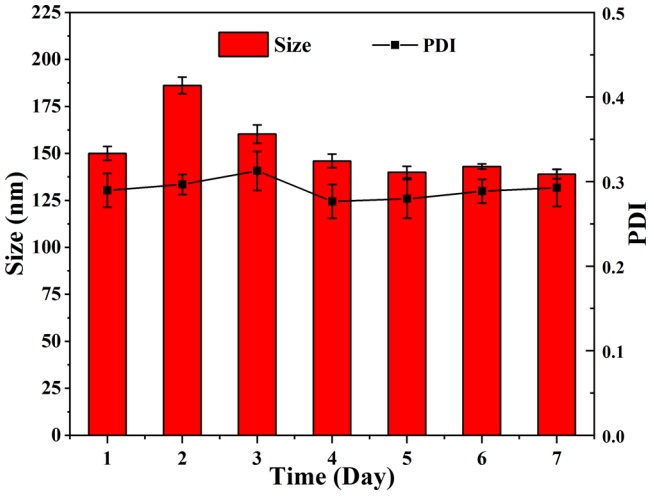

Figure 12. Average size and PDI of CPT nanocrystal-loaded micelles at 37 °C over 1 week.

synthesize PLA-CMCS-g-OA. Specifically, 0.25 g (1.48×10^{-5} mol) of CMCS-g-OA, 0.09 g (7.36×10^{-4} mol) of DMAP, and 0.10 g (4.85×10^{-4} mol) of DCC were mixed with 40 mL of DMSO under constant stirring. The pH of the CMCS-g-OA solution was adjusted to 5.0 using 6.0 M HCl solution, and 0.075 g (3.75×10^{-5} mol) of PLA was added to react with CMCS-g-OA for 48 h. Then, the mixture was centrifuged while the supernatant was freeze-dried. Finally, the lyophilized product (PLA-CMCS-g-OA) was washed with DI water and acetone and dried in a vacuum for further use.

5.3. Critical Micelle Concentration Measurement. Amphiphilic copolymers could form normal-phase micelles in aqueous solutions through spontaneous aggregation. The CMC values of CMCS-g-OA and PLA-CMCS-g-OA in water were determined using an FS-5 fluorescence spectrometer (Edinburgh Instruments, Edinburgh, UK) with pyrene as the probe at the wavelengths of 373 and 384 nm (indicated as I_1 and I_3, respectively, in this work).[57] First, 25.0 μL of pyrene acetone solution (6.0×10^{-6} mol/L) was pipetted into 10 brown flasks, which were immersed in a SHY-A water bath (Chenghui Instruments, Jintan, China) at 40 °C for 1 h. Then, 10.0 mL of polymeric aqueous solutions at different concentrations from 0.001 to 1 mg/mL were added to 10 brown flasks, respectively. After this, the solutions were kept in an ultrasonic apparatus at 25 °C for 24 h. Finally, the polymer solutions were scanned from 350 to 500 nm with a fluorescence spectrometer under an excitation wavelength of 330 nm.[58]

5.4. Preparation of Blank Micelles. First, 100 mg of CMCS-g-OA or PLA-CMCS-g-OA was dissolved in 5 mL of DMSO. Then, the polymer−DMSO solutions were diluted using 50 mL of DI water under a stirring of 650 rpm for 2 h. Finally, the resultant solutions were centrifuged to obtain the "wet" micelles after the supernatants were removed.

5.5. Solubility Determination. The solubility of CPT in DMF and the mixed solvents of DMSO/H_2O at 25 °C were measured according to our previous method.[31,59] The

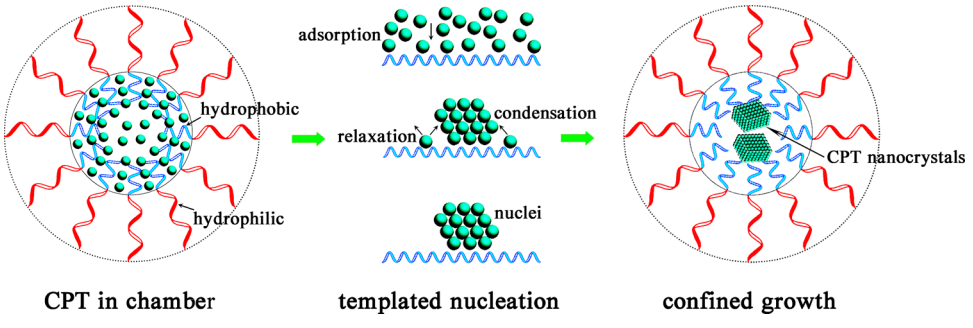

Figure 13. Schematic diagram of mt-ASC.

https://doi.org/10.1021/acsomega.2c01792
ACS Omega 2022, 7, 21000−21013

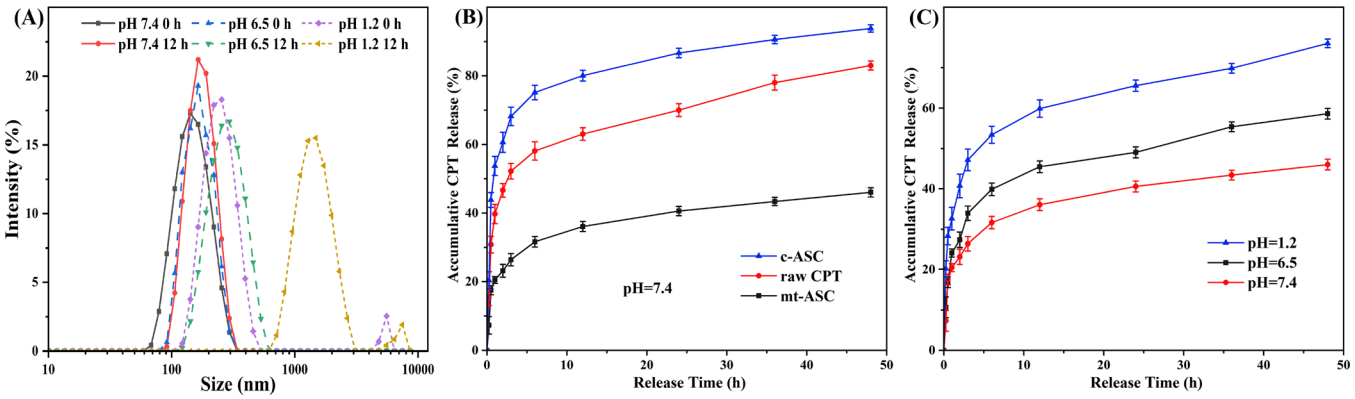

Figure 14. Average size of CPT-loaded micelles in PBS with (A) different pH, in vitro CPT release of raw material, c-ASC, and mt-ASC products in PBS at (B) pH 7.4 and mt-ASC products in PBS at (C) pH 1.2, 6.5, and 7.4.

Scheme 1. Syntheses of PLA-CMCS-g-OA

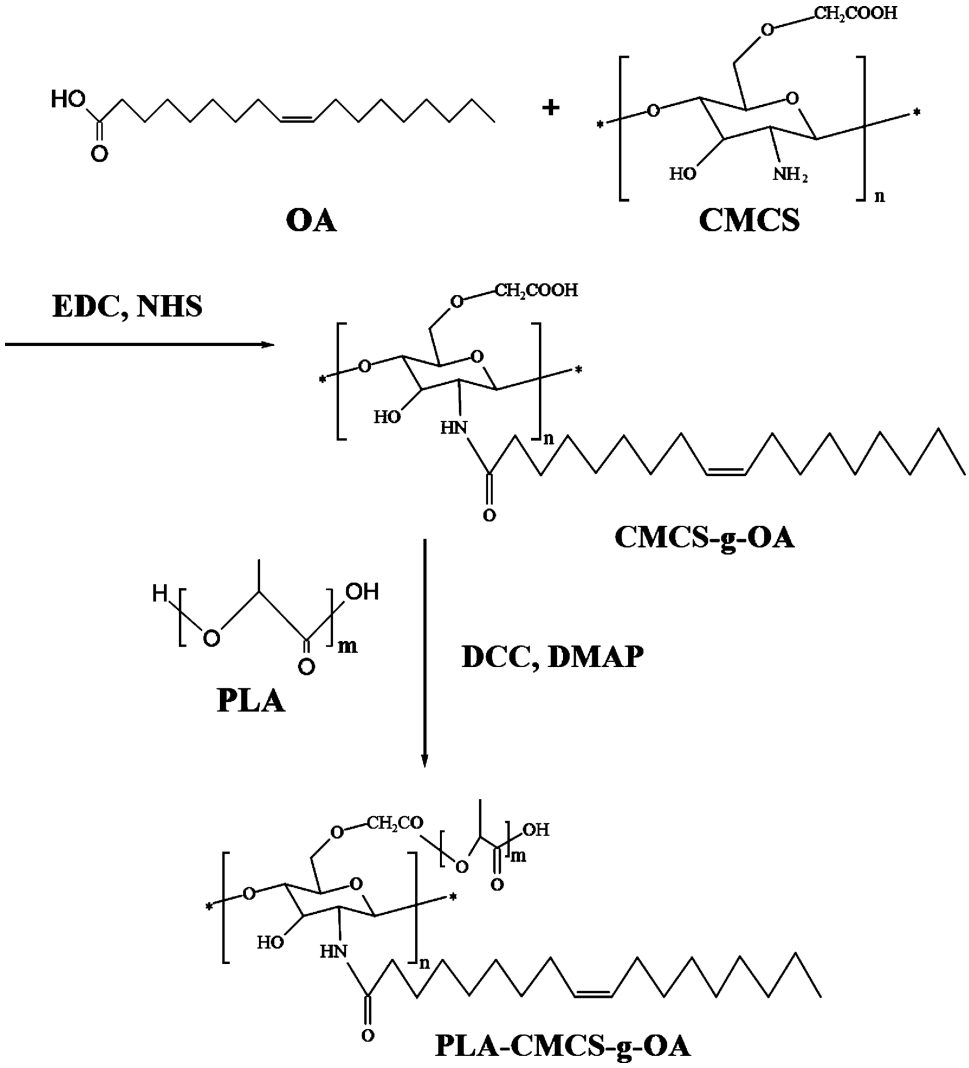

compositions of DMSO in DMSO/H_2O mixtures were 100, 80, 60, 50, 40, 20, and 0 wt %, respectively. The residual solids in equilibrium with the solutions were analyzed by XRD for their crystalline nature. Each group of experiments was performed in parallel three times, and the solubility data reported were the average values.

5.6. Preparation of CPT-Loaded Micelles. First, the PLA-CMCS-g-OA micelles obtained earlier were added to the saturate CPT solutions at 25 °C under a stirring of 650 rpm until the CPT concentration in bulk solutions remained stable. Then, the mixtures were centrifuged to obtain the CPT-loaded micelles after the supernatant was removed.

https://doi.org/10.1021/acsomega.2c01792
ACS Omega 2022, 7, 21000−21013

The CPT concentration in bulk solutions was monitored with a TU-1901 UV spectrophotometer (Persee, Beijing, China) at 367 nm, using a preconstructed standard curve. The CPT LC of PLA-CMCS-g-OA micelles was calculated using the following equations.[28]

$$\mathrm{LC}(\%) = \frac{V(C_0 - C_E)}{m_{\mathrm{micelles}}} \times 100\% \quad (3)$$

where V refers to the volume of CPT saturated solution, C_0 is the initial concentration of CPT in the saturated solution, C_E is the equilibrium concentration of CPT in the supernatant, and m_{micelles} is the weight of added micelles.

5.7. Antisolvent Crystallization. CPT nanocrystals were prepared through c-ASC and mt-ASC at room temperature. For the c-ASC method, 10 mL of DMSO solutions of CPT at 10 mg/mL were drawn into ca. 100 mL of DI water at 2 mL/min and with a linear addition, respectively, through a constant pressure dropping funnel, which was debugged before the antisolvent crystallization experiments. After being agitated for 1 h, the precipitates were harvested and placed in an oven at 30 °C for drying over 48 h to obtain dried products.

In mt-ASC, about 480 mg of CPT-loaded micelles were dispersed into ca. 100 mL of DI water under stirring. After 24 h, the micelles were collected with 0.1 μm filters. Finally, the obtained CPT cake was dried at 30 °C for 48 h to obtain micelle-capsulated CPT nanocrystals.

5.8. Characterization of Amphiphilic Polymers. The FTIR spectra of CMCS, OA, CMCS-g-OA, PLA, and PLA-CMCS-g-OA were collected with a 650S spectrophotometer (Gangdong Sci. & Tech., Tianjin, China) with the aid of KBr. The scanning wavenumber ranged from 400 to 4000 cm^{-1}. The ^{1}H NMR spectra of CMCS, OA, CMCS-g-OA, PLA, and PLA-CMCS-g-OA were obtained using a WNMR-I-600 M spectrometer (Qone Instruments, Wuhan, China).[60] An LC15RI GPC system (HMC Instruments, Suzhou, China) was used to determine the molecular weights of CMCS-g-OA and PLA-CMCS-g-OA. PL gel Olexis (7.5 × 300 mm) as a column, THF as the eluent with a flow rate of 1 mL/min at 40 °C, and a differential refractive index detector were used. Meanwhile, the calibration was performed using polysaccharides as a standard sample.[61] The thermal analyses of CMCS, CMCS-g-OA, and PLA-CMCS-g-OA were carried out with a ZRT-B thermogravimetric analyzer (Jingyi Gaoke Instruments, Beijing, China). The 5 mg sample was poured into a pinhole aluminum crucible and heated from room temperature to 600 °C under a nitrogen atmosphere at 10 °C/min.[27]

5.9. Characterization of Polymer Micelles. The morphologies of blank and CPT-loaded micelles were identified using TEM. First, a few drops of sample were dipped on a copper net, followed by being naturally dried. Then, the dried sample was dyed with a 2% phosphotungstic acid aqueous solution. Finally, the dyed sample was scrutinized with a Tecnai G2 20 TEM (FEI, Hillsboro, OH).[62]

The stability of blank micelles and CPT nanocrystal-loaded micelles in vitro under different storage temperatures was characterized through the change of their zeta potential and PSD for a fixed period. First, the micelle stock solution was stored at 4 or 37 °C, respectively. Then, a certain volume of solution was sampled every 24 h for PSD and zeta potential measurements using a ZEN 3690 DLS system (Malvern Instruments, Malvern, UK). Each measurement was repeated three times.[63]

The disassembly of CPT-loaded micelles triggered by pH was investigated by monitoring the change of their size. Briefly, CPT-loaded micelles of 1 mg/mL were incubated in buffer solution at pH 1.2, 6.5, and 7.4. After incubation in a 37 °C thermostatic shaking bed at 150 rpm for 12 h, the size distribution of the micelles was measured by DLS.[48]

5.10. Characterization of Crystallization Products. The PXRD diffractograms of raw CPT and products from c-ASC and mt-ASC were obtained from a TD-3700 diffractometer with Cu Kα radiation (Tongda Instruments, Dandong, China).[31]

The morphologies of raw CPT and c-ASC products were obtained using scanning electron microscopy (SEM). The powder samples were first scattered on the conductive glue. Then, they were deposited by the vapor of gold. Finally, the gold-coated samples were observed using a Gemini 300 SEM system (Zeiss, Oberkochen, Germany).[64] As to the products from mt-ASC, their morphologies were observed by TEM as described in Section 5.9.

5.11. Release Experiment. The in vitro release behaviors of raw CPT and the products from c-ASC and mt-ASC were studied in a series of PBS at different pH under 37 °C. In brief, a certain amount of solid sample (m_0) was quickly scattered in an appropriate volume of dispersing agent, and the suspension was moved to a dialysis bag (MWCO 2500 Da), which was presoaked in 100.0 mL of PBS. After this, the aliquots (V_e, 4.0 mL) of buffer solution were withdrawn at intervals, and then, an UV-5500 spectrometer (Metash Instruments, Shanghai, China) was used for measuring the concentration of CPT in the solution at 358 nm. Meanwhile, fresh PBS was continually supplemented so as to maintain the volume of buffer solution (V_0, 100.0 mL) constant. The cumulative release (E) was calculated as[65]

$$E(\%) = \frac{V_0 C_n + V_e \sum_1^{n-1} C_{n-1}}{m_0} \times 100\% \quad (4)$$

where C_n (mg/mL) refers to the concentration of CPT at the nth time.

5.12. Statistical Analysis. All experiments were repeated three times, and the variance analysis for all measured data was carried out using the statistical software PAST 2.14. When the statistical significance P of each measurement was less than 0.05, the average value and standard deviation were then calculated using Origin 2018 software and finally reported.

■ ASSOCIATED CONTENT

Supporting Information

The Supporting Information is available free of charge at https://pubs.acs.org/doi/10.1021/acsomega.2c01792.

GPC spectra of CMCS-g-OA and PLA-CMCS-g-OA (Figure S1); diffractograms of the raw material and the remaining crystals after liquid−solid equilibria (Figure S2); and standard curve of CPT in DMF (Figure S3) (PDF)

■ AUTHOR INFORMATION

Corresponding Author

Jie Lu − *Chemical Engineering Department, Frontier Medical Technologies Institute, Shanghai University of Engineering*

https://doi.org/10.1021/acsomega.2c01792
ACS Omega 2022, 7, 21000−21013

Science, Shanghai 201620, China; orcid.org/0000-0002-4581-2032; Email: lujie@sues.edu.cn

Authors

Jianghao Zhang − *Chemical Engineering Department, Frontier Medical Technologies Institute, Shanghai University of Engineering Science, Shanghai 201620, China*

Boxuan Lou − *Chemical Engineering Department, Frontier Medical Technologies Institute, Shanghai University of Engineering Science, Shanghai 201620, China*

Xiaolan Qin − *Chemical Engineering Department, Frontier Medical Technologies Institute, Shanghai University of Engineering Science, Shanghai 201620, China*

Yinwen Li − *Materials Science & Engineering School, Linyi University, Linyi 276000, China;* orcid.org/0000-0003-2929-6223

Haikuan Yuan − *Chemical Engineering Department, Frontier Medical Technologies Institute, Shanghai University of Engineering Science, Shanghai 201620, China*

Lijuan Zhang − *Chemical Engineering Department, Frontier Medical Technologies Institute, Shanghai University of Engineering Science, Shanghai 201620, China*

Xijian Liu − *Chemical Engineering Department, Frontier Medical Technologies Institute, Shanghai University of Engineering Science, Shanghai 201620, China;* orcid.org/0000-0001-5856-9142

Yan Zhang − *Process Engineering Department, Memorial University of Newfoundland, St John's, NL A1B 3X5, Canada;* orcid.org/0000-0003-0107-1014

Complete contact information is available at: https://pubs.acs.org/10.1021/acsomega.2c01792

Author Contributions

‖J.Z. and B.L. contributed equally to this work.

Notes

The authors declare no competing financial interest.

■ ACKNOWLEDGMENTS

We appreciate the National Natural Science Foundation of China (Nos. 21978165, 22081340412, 22078191, 22172070, and 92156020) for supporting this work.

■ REFERENCES

(1) Saha, S.; Mishra, A. A facile preparation of rutin nanoparticles and its effects on controlled growth and morphology of calcium oxalate crystals. *J. Cryst. Growth* **2020**, *540*, No. 125635.

(2) Mohammadi, H. S.; Asl, A. H.; Khajenoori, M. Solubility measurement and preparation of nanoparticles of ampicillin using subcritical water precipitation method. *Korean J. Chem. Eng.* **2021**, *38*, 2304−2312.

(3) Liu, T.; Yao, G.; Zhang, X.; Zuo, X.; Wang, L.; Yin, H.; Moschwitzer, J. P. Systematical investigation of different drug nanocrystal technologies to produce fast dissolving meloxicam tablets. *AAPS PharmSciTech* **2018**, *19*, 783−791.

(4) Huang, Y.; Jiang, Y.; Yang, X. R.; Ren, Y.; Zhan, D.; Cölfen, H.; Hou, Z. Q.; Liu, X. Y. Direct growth of microspheres on amorphous precursor domains in polymer-controlled crystallization of indomethacin. *Cryst. Growth Des.* **2016**, *16*, 1428−1434.

(5) Fontana, F.; Figueiredo, P.; Zhang, P.; Hirvonen, J. T.; Liu, D.; Santos, H. A. Production of pure drug nanocrystals and nano co-crystals by confinement methods. *Adv. Drug Delivery Rev.* **2018**, *131*, 3−21.

(6) Witika, B.; Aucamp, M.; Mweetwa, L.; Makoni, P. Application of fundamental techniques for physicochemical characterizations to understand post-formulation performance of pharmaceutical nanocrystalline materials. *Crystals* **2021**, *11*, 310.

(7) Witika, B. A.; Smith, V. J.; Walker, R. B. Top-down synthesis of a lamivudine-zidovudine nano co-crystal. *Crystals* **2020**, *11*, 33.

(8) Sinha, B.; Muller, R. H.; Moschwitzer, J. P. Bottom-up approaches for preparing drug nanocrystals: formulations and factors affecting particle size. *Int. J. Pharm.* **2013**, *453*, 126−141.

(9) Xi, Y. M.; Lu, Y. C. Interpretation on a nonclassical crystallization route of prussian white nanocrystal preparation. *Cryst. Growth Des.* **2021**, *21*, 1086−1092.

(10) Yi, T.; Liu, C.; Zhang, J.; Wang, F.; Wang, J. R.; Zhang, J. F. A new drug nanocrystal self-stabilized pickering emulsion for oral delivery of silybin. *Eur. J. Pharm. Sci.* **2017**, *96*, 420−427.

(11) Fan, M. X.; Geng, S. C.; Liu, Y.; Wang, J.; Wang, Y. T.; Zhong, J.; Yan, Z. Q.; Yu, L. Nanocrystal technology as a strategy to improve drug bioavailability and antitumor efficacy for the cancer treatment. *Curr. Pharm. Des.* **2018**, *24*, 2416−2424.

(12) Wu, K.; Wu, H. R.; Dai, T. C.; Liu, X. Z.; Chen, J. F.; Le, Y. Controlling nucleation and fabricating nanoparticulate formulation of sorafenib using a high-gravity rotating packed bed. *Ind. Eng. Chem. Res.* **2018**, *57*, 1903−1911.

(13) Zhang, Z. L.; Le, Y.; Wang, J. X.; Zhao, H.; Chen, J. F. Development of stabilized itraconazole nanodispersions by using high-gravity technique. *Drug Dev. Ind. Pharm.* **2012**, *38*, 1512−1520.

(14) Zhao, Y. X.; Hua, H. Y.; Chang, M.; Liu, W. J.; Zhao, Y.; Liu, H. M. Preparation and cytotoxic activity of hydroxycamptothecin nanosuspensions. *Int. J. Pharm.* **2010**, *392*, 64−71.

(15) Kim, H. J.; Lee, J. Confined nano-crystallization of celecoxib inside porous mannitol. *J. Cryst. Growth* **2015**, *419*, 108.

(16) Warzecha, M.; Guo, R.; Bhardwaj, R. M.; Reutzel-Edens, S. M.; Price, S. L.; Lamprou, D. A.; Florence, A. J. Direct observation of templated two-step nucleation mechanism during olanzapine hydrate formation. *Cryst. Growth Des.* **2017**, *17*, 6382−6393.

(17) Song, S.; You, B.; Zhu, Y.; Lin, Y.; Wu, Y.; Ge, X. Nanocrystal-organic hybrid antifungal agent: high level oriented assembly of zinc hydroxide carbonate nanocrystals in chitosan. *Cryst. Growth Des.* **2013**, *14*, 38−45.

(18) Chen, N. S.; Tong, Z. H.; Yang, W. H.; Brennan, A. B. Biocomposites with tunable properties from poly(lactic acid)-based copolymers and carboxymethyl cellulose via ionic assembly. *Carbohydr. Polym.* **2015**, *128*, 122−129.

(19) Biswas, S.; Kumari, P.; Lakhani, P. M.; Ghosh, B. Recent advances in polymeric micelles for anti-cancer drug delivery. *Eur. J. Pharm. Sci.* **2016**, *83*, 184−202.

(20) Hui, T.; Chen, D.; Jiang, M. A one-step approach to the highly efficient preparation of core-stabilized polymeric micelles with a mixed shell formed by two incompatible polymers. *Macromolecules* **2005**, *38*, 5834−5837.

(21) He, L. M.; Qin, X. Y.; Fan, D. H.; Feng, C. L.; Wang, Q.; Fang, J. Y. Dual-stimuli responsive polymeric micelles for the effective treatment of rheumatoid arthritis. *ACS Appl. Mater. Interfaces* **2021**, *13*, 21076−21086.

(22) Sun, X. S.; Yu, K. T.; Zhou, Y. L.; Dong, S. Y.; Hu, W. J.; Sun, Y. T.; Li, Y. H.; Xie, J.; Lee, R. J.; Sun, F. Y.; Ma, Y. F.; Wang, S. N.; Kim, B. Y. S.; Wang, Y. F.; Yang, Z. G.; Jiang, W.; Li, Y. X.; Teng, L. S. Self-assembled pH-sensitive polymeric nanoparticles for the inflammation-targeted delivery of Cu/Zn-superoxide dismutase. *ACS Appl. Mater. Interfaces* **2021**, *13*, 18152−18164.

(23) Lee, M. K.; Bang, J.; Shin, K.; Lee, J. Fabrication of water-soluble nanocrystals using amphiphilic block copolymer patterned surfaces. *Cryst. Growth Des.* **2010**, *10*, 5187−5192.

(24) Cheng, M.; Liu, Q. M.; Gan, T. T.; Fang, Y. Y.; Yue, P. F.; Sun, Y. B.; Jin, Y.; Feng, J. F.; Tu, L. X. Nanocrystal-loaded micelles for the enhanced in vivo circulation of docetaxel. *Molecules* **2021**, *26*, 4481−4496.

(25) Dai, Y. X.; Wang, S.; Shi, W. B.; Lang, M. D. pH-responsive carboxymethyl chitosan-derived micelles as apatinib carriers for effective anti-angiogenesis activity: preparation and in vitro evaluation. *Carbohydr. Polym.* **2017**, *176*, 107−116.

(26) Kumar, R.; Sirvi, A.; Kaur, S.; Samal, S. K.; Roy, S.; Sangamwar, A. T. Polymeric micelles based on amphiphilic oleic acid modified carboxymethyl chitosan for oral drug delivery of bcs class iv compound: intestinal permeability and pharmacokinetic evaluation. *Eur. J. Pharm. Sci.* **2020**, *153*, No. 105466.
(27) Yang, C. F.; Yuan, C.; Liu, W. Y.; Guo, J. W.; Feng, D. C.; Yin, X. Q.; Lin, W. J.; Shuttleworth, P. S.; Yue, H. B. DPD studies on mixed micelles self-assembled from MPEG-PDEAEMA and MPEG-PCL for controlled doxorubicin release. *Colloids Surf., B* **2019**, *178*, 56−65.
(28) Wang, J. H.; Han, Y. F.; Xu, Z. Y.; Yang, X. Z.; Ramakrishna, S.; Liu, Y. Dissipative particle dynamics simulation: a review on investigating mesoscale properties of polymer systems. *Macromol. Mater. Eng.* **2021**, *306*, No. 2000724.
(29) Yang, C. F.; Liu, W. Y.; Xiao, J. Y.; Yuan, C.; Chen, Y. X.; Guo, J. W.; Yue, H. B.; Zhu, D. Y.; Lin, W. J.; Tang, S. Q.; Dong, X. Y. pH-sensitive mixed micelles assembled from PDEAEMA-PPEGMA and PCL-PPEGMA for doxorubicin delivery: experimental and DPD simulations study. *Pharmaceutics* **2020**, *12*, 170−187.
(30) Yang, C. F.; Yin, L.; Yuan, C.; Liu, W. Y.; Guo, J. W.; Shuttleworth, P. S.; Yue, H. B.; Lin, W. J. DPD simulations and experimental study on reduction-sensitive polymeric micelles self-assembled from PCL-SS-PPEGMA for doxorubicin controlled release. *Colloids Surf., B* **2021**, *204*, No. 111797.
(31) Pi, P. H.; Qin, D. X.; Lan, J. L.; Cai, Z. Q.; Yuan, X. X.; Xu, S. P.; Zhang, L. J.; Qian, Y.; Wen, X. F. Dissipative particle dynamics simulation on the nanocomposite delivery system of quantum dots and poly(styrene-b-ethylene oxide) copolymer. *Ind. Eng. Chem. Res.* **2015**, *54*, 6123−6134.
(32) Kuru, M. M.; Dalgakiran, E. A.; Kacar, G. Investigation of morphology, micelle properties, drug encapsulation and release behavior of self-assembled PEG-PLA-PEG block copolymers: a coarse-grained molecular simulations study. *Colloids Surf., A* **2021**, *629*, No. 127445.
(33) Yang, Z. X.; Zhao, H. Q.; Wang, D. L.; Yin, L.; Cai, K. X.; Lin, Z. H.; Chen, T.; Yang, C. F. DPD simulations on mixed polymeric DOX-loaded micelles assembled from PCL-SS-PPEGMA/PDEA-PPEGMA and their dual pH/reduction-responsive release. *Phys. Chem. Chem. Phys.* **2021**, *23*, 19011−19021.
(34) Bashir, D. J.; Manzoor, S.; Khan, I. A.; Bashir, M.; Agarwal, N. B.; Rastogi, S.; Arora, I.; Samim, M. Nanonization of magnoflorine-encapsulated novel chitosan-collagen nanocapsules for neurodegenerative diseases: in vitro evaluation. *ACS Omega* **2022**, *7*, 6472−6480.
(35) Almeida, A.; Araujo, M.; Novoa-Carballal, R.; Andrade, F.; Goncalves, H.; Reis, R. L.; Lucio, M.; Schwartz, S., Jr.; Sarmento, B. Novel amphiphilic chitosan micelles as carriers for hydrophobic anticancer drugs. *Mater. Sci. Eng., C* **2020**, *112*, No. 110920.
(36) Zhou, C.; Yang, Z. M.; Zhang, L.; Dong, E. M.; He, Z. Y.; Liu, X. W.; Wang, C.; Yang, Y.; Jiao, J.; Liu, Y. H.; Chen, Y.; Li, P. W. Self-assembled nano-vesicles based on mPEG-NH_2 modified carboxymethyl chitosan-graft-eleostearic acid polymers for delivery of spinosad for helicoverpa armigera. *React. Funct. Polym.* **2020**, *146*, No. 104438.
(37) Jena, S. K.; Sangamwar, A. T. Polymeric micelles of amphiphilic graft copolymer of α-tocopherol succinate-g-carboxymethyl chitosan for tamoxifen delivery: synthesis, characterization and in vivo pharmacokinetic study. *Carbohydr. Polym.* **2016**, *151*, 1162−1174.
(38) Changez, M.; Kang, N. G.; Lee, J. S. Uni-molecular hollow micelles from amphiphilic homopolymer poly(2-(4-vinylphenyl)-pyridine). *Small* **2012**, *8*, 1173−1179.
(39) Wang, D. B.; Lu, J.; Zhang, L. L.; Fan, F. F.; Zhang, L. J.; Liu, X. J.; Yuan, H. K.; Zhu, X. Y. Experimental and molecular dynamics simulation study on the primary nucleation of penicillamine racemate and its enantiomers in the mixture solvent of water and ethanol. *Ind. Eng. Chem. Res.* **2020**, *59*, 21957−21968.
(40) Zong, L. L.; Wang, H. Y.; Hou, X. Q.; Fu, L. K.; Wang, P. R.; Xu, H. L.; Yu, W. J.; Dai, Y. X.; Qiao, Y. H.; Wang, X. F.; Yuan, Q.; Pang, X. B.; Han, G.; Pu, X. H. A novel GSH-triggered polymeric nanomicelles for reversing MDR and enhancing antitumor efficiency of hydroxycamptothecin. *Int. J. Pharm.* **2021**, *600*, No. 120528.
(41) Hao, X. F.; Gai, W. W.; Wang, L. N.; Zhao, J. D.; Sun, D. D.; Yang, F.; Jiang, H. X.; Feng, Y. K. 5-Boronopicolinic acid-functionalized polymeric nanoparticles for targeting drug delivery and enhanced tumor therapy. *Mater. Sci. Eng., C* **2021**, *119*, No. 111553.
(42) Malhotra, S.; Dumoga, S.; Joshi, A.; Mohanty, S.; Singh, N. Polymeric micelles coated with hybrid nanovesicles enhance the therapeutic potential of the reversible topoisomerase inhibitor camptothecin in a mouse model. *Acta Biomater.* **2021**, *121*, 579−591.
(43) Lu, N. N.; Xi, L. C.; Zha, Z. S.; Wang, Y. H.; Han, X. H.; Ge, Z. S. Acid-responsive endosomolytic polymeric nanoparticles with amplification of intracellular oxidative stress for prodrug delivery and activation. *Biomater. Sci.* **2021**, *9*, 4613−4629.
(44) Zhang, S. D.; Zhang, X.; Meng, J.; Lu, L.; Du, S. D.; Xu, H. Y.; Wu, S. Z. Study on the effect of polymer excipients on the dispersibility, interaction, solubility, and scavenging reactive oxygen species of myricetin solid dispersion: experiment and molecular simulation. *ACS Omega* **2022**, *7*, 1514−1526.
(45) Wang, J.; Muhammad, N.; Li, T.; Wang, H.; Liu, Y.; Liu, B.; Zhan, H. Hyaluronic acid-coated camptothecin nanocrystals for targeted drug delivery to enhance anticancer efficacy. *Mol. Pharmaceutics* **2020**, *17*, 2411−2425.
(46) Du, J.; Zhou, Y.; Wang, L.; Wang, Y. Effect of PEGylated chitosan as multifunctional stabilizer for deacetyl mycoepoxydience nanosuspension design and stability evaluation. *Carbohydr. Polym.* **2016**, *153*, 471−481.
(47) Adawy, A.; Amghouz, Z.; van Hest, J. C. M.; Wilson, D. A. Sub-micron polymeric stomatocytes as promising templates for confined crystallization and diffraction experiments. *Small* **2017**, *13*, No. 1700642.
(48) Li, M.; Zhang, L.; Xuan, Y.; Zhi, D. F.; Wang, W.; Zhang, W. J.; Zhao, Y. N.; Zhang, S. F.; Zhang, S. B. pH-sensitive hyaluronic acid-targeted prodrug micelles constructed via a one-step reaction for enhanced chemotherapy. *Int. J. Biol. Macromol.* **2022**, *206*, 489−500.
(49) Wen, W.; Guo, C.; Guo, J. Acid-responsive adamantane-cored amphiphilic block polymers as platforms for drug delivery. *Nanomaterials* **2021**, *11*, 188.
(50) Xing, T.; Yan, L. pH-responsive amphiphilic block copolymer prodrug conjugated near infrared fluorescence probe. *RSC Adv.* **2014**, *4*, 28186−28194.
(51) Li, Y. W.; Lu, H. Z.; Liang, S. M.; Xu, S. F. Dual stable nanomedicines prepared by cisplatin-crosslinked camptothecin prodrug micelles for effective drug delivery. *ACS Appl. Mater. Interfaces* **2019**, *11*, 20649−20659.
(52) Zheng, P.; Liu, Y.; Chen, J.; Xu, W.; Li, G.; Ding, J. Targeted pH-responsive polyion complex micelle for controlled intracellular drug delivery. *Chin. Chem. Lett.* **2020**, *31*, 1178−1182.
(53) Gao, J. L.; Xu, Y.; Zheng, Y.; Wang, X.; Li, S. T.; Yan, G. Q.; Wang, J.; Tang, R. P. pH-sensitive carboxymethyl chitosan hydrogels via acid-labile ortho ester linkage as an implantable drug delivery system. *Carbohydr. Polym.* **2019**, *225*, No. 115237.
(54) Wang, Y.; Qin, F.; Tan, H.; Zhang, Y.; Jiang, M.; Lu, M.; Yao, X. pH-responsive glycol chitosan-cross-linked carboxymethyl-beta-cyclodextrin nanoparticles for controlled release of anticancer drugs. *Int. J. Nanomed.* **2015**, *10*, 7359−7369.
(55) Zhang, H.; Hollis, C. P.; Zhang, Q.; Li, T. Preparation and antitumor study of camptothecin nanocrystals. *Int. J. Pharm.* **2011**, *415*, 293−300.
(56) Feng, Y. H.; Zhang, X. P.; Hao, Y. Y.; Ren, G. Y.; Guo, X. D. Simulation study of the pH sensitive directed self-assembly of rheins for sustained drug release hydrogel. *Colloids Surf., B* **2020**, *195*, No. 111260.
(57) Wang, X. Y.; Guo, Y. L.; Qiu, L. Z.; Wang, X. Y.; Li, T. L.; Han, L. F.; Ouyang, H. Z.; Xu, W.; Chu, K. D. Preparation and evaluation of carboxymethyl chitosan-rhein polymeric micelles with synergistic antitumor effect for oral delivery of paclitaxel. *Carbohydr. Polym.* **2019**, *206*, 121−131.

https://doi.org/10.1021/acsomega.2c01792
ACS Omega 2022, 7, 21000−21013

(58) Zhang, M. N.; Zhang, S. J.; Zhang, K.; Zhu, Z. Y.; Miao, Y. L.; Qiu, Y. D.; Zhang, P. K.; Zhao, X. B. Self-assembly of polymer-doxorubicin polymers to form polyprodrug micelles for pH/enzyme dual-responsive drug delivery. *Colloids Surf., A* **2021**, *622*, No. 126669.
(59) Fan, F. F.; Yuan, H. K.; Feng, Y. H.; Liu, F. J.; Zhang, L. J.; Liu, X. J.; Zhu, X. Y.; An, W.; Rohani, S.; Lu, J. Molecular simulation approaches for the prediction of unknown crystal structures and solubilities of (R)- and (R,S)-crizotinib in organic solvents. *Cryst. Growth Des.* **2019**, *19*, 5882−5895.
(60) Luo, Z. L.; Li, Y.; Wang, B. B.; Jiang, J. W. pH-sensitive vesicles formed by amphiphilic grafted copolymers with tunable membrane permeability for drug loading/release: a multiscale simulation study. *Macromolecules* **2016**, *49*, 6084−6094.
(61) Bagheri, M.; Bigdeli, E.; Pourmoazzen, Z. Self-assembled micellar nanoparticles of a novel amphiphilic cholesteryl-poly(L-lactic acid)-b-poly(poly (ethylene glycol)methacrylate) block-brush copolymer. *Iran. Polym. J.* **2013**, *22*, 293−302.
(62) Ahmad, M.; Nawaz, T.; Assiri, M. A.; Hussain, R.; Hussain, I.; Imran, M.; Ali, S.; Wu, Z. Fabrication of bimetallic Cu-Ag nanoparticle-decorated poly(cyclotri phosphazene-co-4,4′-sulfonyldiphenol) and its enhanced catalytic activity for the reduction of 4-nitrophenol. *ACS Omega* **2022**, *7*, 7096−7102.
(63) Gomes, D. S.; da Costa, A.; Pereira, A. M.; Casal, M.; Machado, R. Biocomposites of silk-elastin and essential oil from mentha piperita display antibacterial activity. *ACS Omega* **2022**, *7*, 6568−6578.
(64) Jin, Y. H.; Hu, H. Y.; Qiao, M. X.; Zhu, J.; Qi, J. W.; Hu, C. J.; Zhang, Q.; Chen, D. W. pH-sensitive chitosan-derived nanoparticles as doxorubicin carriers for effective anti-tumor activity: preparation and in vitro evaluation. *Colloids Surf., B* **2012**, *94*, 184−191.
(65) Long, L. X.; Zhao, J.; Li, K.; He, L. G.; Qian, X. M.; Liu, C. Y.; Wang, L. M.; Yang, X. Q.; Sun, J.; Ren, Y.; Kang, C. S.; Yuan, X. B. Synthesis of star-branched PLA-b-PMPC copolymer micelles as long blood circulation vectors to enhance tumor-targeted delivery of hydrophobic drugs in vivo. *Mater. Chem. Phys.* **2016**, *180*, 184−194.

https://doi.org/10.1021/acsomega.2c01792
ACS Omega 2022, 7, 21000−21013